NSF Grant # 0826276
NSF PROGRAM NAME: Dynamical Systems

Exploiting Parametric Effects in Resonant Nanosystems

Jeffrey F. Rhoads[PI]
School of Mechanical Engineering and Birck Nanotechnology Center, Purdue University
contact email: jfrhoads@purdue.edu

William G. Conley, Arvind Raman[Co-PI]
School of Mechanical Engineering and Birck Nanotechnology Center, Purdue University

Charles M. Krousgrill
School of Mechanical Engineering, Purdue University

Lin Yu
Department of Physics and Birck Nanotechnology Center, Purdue University

Saeed Mohammadi[Co-PI]
School of Electrical Engineering and Birck Nanotechnology Center, Purdue University

Abstract: This work examines the nonlinear dynamics of suspended, electrostatically-actuated single-walled carbon nanotube resonators. Specifically, the work considers the near-resonant response of these systems under combined parametric and direct excitation, and explores the relative importance of each excitation mechanism in a prototypical device. Given the preliminary nature of this work, AUTO simulations are used to capture the salient features of the nanoresonator's nonlinear response. Ongoing fabrication and characterization efforts, aimed at validating predicted dynamic behaviors, are also described.

1. Introduction: Recently, resonant nanoscale electromechanical systems (NEMS) have garnered appreciable attention due to their ability to manipulate signals with GHz frequencies [1] and detect chemical substances with zeptogram mass sensitivity [2]. In general, NEMS provide many advantages over their traditional counterparts, including higher natural frequencies, lower power consumption, and improved compatibility with CMOS fabrication techniques. Nanoscale mechanical resonators also provide a useful replacement to traditional circuit elements due to their superior fundamental noise characteristics. In prior works, a number of distinct suspended, single-walled carbon nanotube (SWCNT) resonators have been successfully fabricated and characterized [1, 3, 4]. A key result of prior work is the applicability of thin beam theory to SWCNT based resonators. In particular, it has been reported that as long as the stress at the clamped edges of a suspended CNT does not buckle the tube, continuum mechanics are capable of accurately capturing the behavior of the device [5].

In prior work [6] the authors' have explained the onset of non-planar motions in nanoscale resonators, which are attributable to the symmetry of the device. These non-planar motions occur as a direct result of the nanotube stretching as it deforms. The present work seeks to build upon the results of [1, 3, 4, 6], by considering the near resonant response of a representative device with a physically-consistent model of the electrostatic force [7, 8]. This refined model introduces linear and nonlinear parametric excitation to the system, as well as their attendant resonances.

In the system of interest parametric excitation serves to modulate the stiffness of the resonator. At particular parametric excitation amplitudes and frequencies, large amplitude motion is known to occur [9]. While parametric excitation in linear equations is well understood [10], the interaction of parametric excitation with physically-relevant nonlinearities has not been fully explored. Recently, planar problems have been considered at the microscale (see for example [11, 12]). At the nanoscale, only structural nonlinearities have been

included in prior models of suspended resonators [6]; it is worth noting that parametric excitation of cantilevered nanostructures has previously been examined [7, 13, 14]. This preliminary work examines the impact of parametric excitation on the model previously considered in [6].

2. Model: A sketch of a representative CNT oscillator is shown in Fig. 1. Here an oscillator of diameter d and length L is suspended over a trench of height h. The horizontal deflection of the device is defined to be v, and the vertical deflection is defined to be w. Following the nondimensionalization procedure of [6] results in the following coupled equations:

$$\begin{aligned} &W_{,\tau\tau} + \frac{1}{Q}W_{,\tau} + \frac{1}{\beta^4}W_{,XXXX} \\ &= \frac{1}{2R^2\beta^4}W_{,XX}\int_0^1 \left[W_{,X}^2 + V_{,X}^2\right] dX + F(X,\tau) \\ &V_{,\tau\tau} + \frac{1}{Q}V_{,\tau} + \frac{1}{\beta^4}V_{,XXXX} \\ &= \frac{1}{2R^2\beta^4}V_{,XX}\int_0^1 \left[W_{,X}^2 + V_{,X}^2\right] dX. \end{aligned} \tag{1}$$

Note that W is the dimensionless vertical deflection, V is the horizontal deflection, R is the radius of gyration, and β is a function of the eigenmode of oscillation. Spatial partial derivatives are denoted as $(\cdot)_{,X}$, while temporal partial derivatives are $(\cdot)_{,\tau}$. Dissipation, attributable to clamping losses and gas damping, is captured by a quality factor Q. The nondimensional force per unit length, $F(X,\tau)$, is proportional to the capacitance between the CNT and gate electrode, as well as the voltage difference, $V_g(\tau)$ [4, 6]. Assuming small vibration amplitudes and minimal fringe field effects, the force is expanded in a Taylor series about $W = 0$ yielding

$$\begin{aligned} F(X,\tau) &= -\frac{S\pi\epsilon_0 V_g^2(\tau)}{h^2}\frac{1}{(1+W)[\ln(4(1+W)/D)]^2} \\ &\approx -\frac{S\pi\epsilon_0 V_g^2(\tau)}{h^2}\left[f_0 - f_1 W + f_2 W^2 - f_3 W^3\right], \end{aligned} \tag{2}$$

where ϵ_0 is the permittivity of free space and $S = \frac{L^4}{\beta^4 EI}$ is the compliance of the oscillator. The coefficients f_n $(n = 0, 1, 2, 3)$ are shown in Table 1.

Performing a single-mode Galerkin projection on Eq. (1) where the eigenmode, $\phi(X)$, is the fundamental mode of a linear clamped-clamped oscillator ($\beta = 4.73$) [15] results in the following lumped parameter model:

$$\begin{aligned} &q_{1,\tau\tau} + \frac{1}{Q}q_{1,\tau} + q_1 + 8\alpha q_1[q_1^2 + q_2^2] = \\ &\qquad - V_g^2(\tau)[F_0 - F_1 q_1 + F_2 q_1^2 - F_3 q_1^3] \\ &q_{2,\tau\tau} + \frac{1}{Q}q_{2,\tau} + q_2 + 8\alpha q_2[q_1^2 + q_2^2] = 0. \end{aligned} \tag{3}$$

Here, the in-plane displacement is defined to be $q_1(\tau)$ and the out-of-plane displacement is denoted as $q_2(\tau)$. Likewise, the nonlinear stiffness coefficient is taken to be $\alpha = \frac{1}{16R^2\beta^4}[\int_0^1 \phi_{,X}^2\, dX]^2$. The electrostatic forcing coefficients F_n are shown in Table 1.

Previous works [4] have adopted an applied voltage form given by $V_g = V_{dc} + V_{ac}\sin(\Omega\tau)$. This excitation mechanism intrinsically results in degenerate multiple frequency excitation in Eq. (3). The complexity of this model may be reduced when $V_{dc} \gg V_{ac}$, yielding the harmonic excitation $V_g^2 \approx 2V_{dc}V_{ac}\sin(\Omega\tau)$. It should be noted that, the dynamic consequences of V_{dc}^2 are neglected in these works and is assumed to merely increases the natural frequency of the resonator. The present effort begins by examining this model. Though the aforementioned assumption appears reasonable under certain conditions, prior works have not rigorously demonstrated that tensioning does not substantially modify the dynamics of a given CNT resonator. Accordingly, this work also examines the dynamic response of a representative device excited by a voltage excitation signal of the form $V_g(\tau) = \sqrt{V_{dc}^2 + V_{ac}^2\sin(\Omega\tau)}$. This voltage signal, previously used in [16], is periodic and results in harmonic forcing in Eq. (3).

3. Simulation Results: Given the complexity of Eq. (3), the equation is simulated in AUTO [17], a powerful computational tool for finding bifurcations of solution branches of nonlinear differential equations. This approach serves to guide both ongoing analytical investigations of pertinent dynamical behavior and the predictive design of functional devices. In the present effort a 2.5nm diameter, 1 μm long SWCNT is considered. The natural frequency of this representative device is 5.02MHz with quality factor $Q = 25$. The nonlinear stiffness coefficient is $\alpha = 3023$ and the linear compliance is $S = 0.167$ m^2/N. These parameter values are typical of the devices discussed in Section 4; additionally, these parameter values match device 2 of [4] and were examined in [6]. Table 1 shows the computed forcing coefficients, f_n and F_n, for a trench depth of $h = 100$nm.

Table 1: Analytical and computed values of the forcing parameters. The parameter values are discussed in Section 3. Note that a 100nm deep trench is considered here.

f_n in Eq. (2)	f_n	F_n in (3)	F_n $(1/V^2)$
$f_0 = \dfrac{1}{[\ln(4/D)]^2}$	0.0388	$F_0 = \dfrac{1}{S\pi\epsilon_0} 2h^2 f_0 \int_0^1 \phi dX$	7.50
$f_1 = \dfrac{\ln(4/D)+2}{\ln(4/D)^3}$	0.0541	$F_1 = \dfrac{S\pi\epsilon_0}{2h^2} f_1 \int_0^1 \phi^2 dX$	12.6
$f_2 = \dfrac{\ln(4/D)^2 + 3\ln(4/D) + 3}{\ln(4/D)^4}$	0.0663	$F_2 = \dfrac{S\pi\epsilon_0}{2h^2} f_2 \int_0^1 \phi^3 dX$	20.5
$f_3 = \dfrac{3\ln(4/D)^3 + 11\ln(4/D)^2 + 18\ln(4/D) + 12}{3\ln(4/D)^5}$	0.0771	$F_3 = \dfrac{1}{S\pi\epsilon_0} 2h^2 f_3 \int_0^1 \phi^4 dX$	33.2

To characterize and compare the effects of including parametric excitation in our model, three distinct force models are considered: (i) external forcing with linear, quadratic, and cubic parametric excitation, the F_n values are shown in Table 1; (ii) external forcing only ($F_1 = F_2 = F_3 = 0$); and (iii) linear and cubic parametric excitation only ($F_0 = F_2 = 0$). Note that purely-parametric excitation is realizable in CNT resonators by using a symmetric dual gate structure, similar to the electrostatically-excited MEMS resonators of [18].

The in-plane and out-of-plane response of the representative device detailed above is presented in Figs. 2 and 3 for $V_g^2 \approx 2V_{dc}V_{ac}\sin(\Omega\tau)$. Specifically, $V_{dc} = 200$mV is fixed in all of the subfigures while V_{ac} is varied. It is observed that there are only negligible changes in the nonlinear frequency response when the parametric excitation terms are retained, as compared to external forcing. In particularly, when only parametric excitation is considered, the amplitudes of motion are approximately one sixth as large as those obtained with external forcing. In fact, external forcing, under moderate excitation voltages, dominates the response, even when small gate dimensions are considered. This supports the conclusion that the system's dynamic response is dominated by stretching.

To help characterize the effects of parametric excitation on the system's response, it is prudent to map the Arnold tongue in the excitation voltage-excitation frequency parameter space, see Fig. 6. This map is formed by tracking the onset of nontrivial solutions in the purely-parametric problem for $V_g^2 \approx 2V_{dc}V_{ac}\sin(\Omega\tau)$. As seen in prior works [18], as the voltage increases, the bandwidth of the Arnold tongue also increases. Furthermore, as observed in Fig. 2, once the trivial solution loses stability, large amplitudes oscillations occur over a relatively large excitation frequency bandwidth. This parameter space also highlights that a critical excitation voltage which must be exceeded to obtain primary parametric resonance.

Using Fig. 6 for guidance, the dynamic response the in-plane and out-of-plane response of the representative device detailed above was examined again via AUTO simulation. Figures 4 and 5 depict the nonlinear frequency response recovered from the device with $V_g = \sqrt{V_{dc}^2 + V_{ac}^2 \sin(\Omega\tau)}$. As before, $V_{dc} =$ 200mV in each simulation, while V_{ac} is selected to match the force amplitudes utilized in Figs. 2 and 3. Not surprisingly, additional bifurcations and solutions branches arise as a direct result of including the DC tensioning term in the model. Several noteworthy features are displayed in Fig. 4. First, the linear natural frequency increases to $\Omega \approx 9$; this is a direct result of frequency tuning attributable to DC tensioning. Additionally, the backbone curve of the primary resonance shows an initial softening. This softening is also attributable to stretching interacting with the asymmetric stiffness potential formed for small vibration amplitudes [19]. An additional period-2 solution is observed near $\Omega \approx 11$ which is directly attributable to external forcing. Examining this bifurcation requires additional analysis, likely using the method of first-order averaging. The non-planar solution branches shown in Fig. 5 are also increasingly complex. By including the parametric terms as well as DC tensioning, the bifurcation points shift substantially when compared to prior works [6]. Finally, the robust period-1 non-planar branch observed in Figs. 2 and 3 is no longer present in Figs. 4 and 5. This may be an artifact of the numerical implementation in AUTO or a result of the resonance bandwidths no longer overlapping for the in-plane and out-of-plane mode.

The bifurcations and resulting solution branches detailed above, recovered using realistic device parameters, are mathematically interesting and, with

careful analysis, exploitable in practical application. Despite the complexity of the reported dynamics, several consequences are of particular note. First, this work demonstrates that the DC tensioning of a CNT resonator results in additional bifurcations, and thus the tuning of these devices is not as simple as posited by others [4]. Furthermore, the work displays that parametric effects are minimal under moderate excitation voltages. However, with smaller gate dimensions, larger excitation voltages, or higher quality factors parametric effects can be expected to dominate the response.

4. Device Fabrication: It should be noted that suspended CNT resonators are being fabricated concurrently with the previously described computational effort. Using thermal chemical vapor deposition with methane, single-walled carbon nanotubes are selectively synthesized from patterned iron catalysts on a high-resistivity Si substrate coated with an 800nm thermal SiO_2 layer. The resulting CNTs have a diameter of 1-5nm with an approximate spatial density of 0.5 tubes/μm. Metal electrodes (contacts and gates) are defined using a single-step, e-beam lithography process, followed by e-beam evaporation of Cr/Au and lift-off. Trenches are formed beneath the nanotubes by wet-etching the oxide layer; and the CNTs are subsequently released through the use of critical point drying. Figure 7 shows a FESEM of a prototypical device. Note that the suspended length of the nanotube resonator shown herein is approximately 2μm and the effective gap between the gate electrode and the device is approximately 300nm.

The frequency response of these devices is being carefully examined using the measurement set-up shown schematically in Fig. 7. This experimental endeavor is the first to directly measure the motion of a CNT resonators without utilizing signal mixing [4, 1, 3]. It should be noted that this measurement depends on the use of a very high frequency lock-in amplifier (Stanford Research Systems SR844) which enables the direct measurement of the frequency response up to 200MHz. This capability is more than adequate for SWCNT devices with lengths of approximately 1 micron.

5. Conclusions: As noted in the introduction, resonant nanoscale electromechanical systems (NEMS) have garnered appreciable attention due to their ability to manipulate signals with GHz frequencies [1] and detect chemical substances with zeptogram mass sensitivity [2]. This work examines the nonlinear dynamics of a particular class of suspended, electrostatically-actuated single-walled carbon nanotube resonator. The near-resonant response of these systems under combined parametric and direct excitation was examined, and salient response features, potentially exploitable in practical application, have been identified. Though the results detailed in this work are preliminary, they show that the nonlinear response of prototypical devices are appreciably more complex than previously reported, and that careful modeling and analysis must be performed for predictive design. Ongoing efforts are aimed at extended the results detailed herein, accounting for stochastic excitations, and experimentally validating the predicted dynamic behaviors.

Acknowledgements: The authors acknowledge support from the National Science Foundation NIRT Grant No. CCF-05-6660 and Grant 0826276.

Bibliography:

[1] H B Peng, C W Chang, S Aloni, T D Yuzvinsky, and A Zettl. Ultrahigh frequency nanotube resonators. *Physical Review Letters*, 97:087203, 2006.

[2] K. Jensen, K. Kim, and A. Zettl. An atomic-resolution nanomechanical mass sensor. *Nature Nanotechnology*, 3(9):533–537, 2008.

[3] B Witkamp, M Poot, and S J van der Zant. Bending-mode vibration of a suspended nanotube resonator. *Nano Letters*, 6:2904–2908, 2006.

[4] V Sazonova, Y Yaish, H Ustunel, D Roundy, T A Arias, and P McEuen. A tunable carbon nanotube electromechanical oscillator. *Nature*, 431:284–287, 2004.

[5] M Dequesnes, Z Tang, and N R Aluru. Static and dynamic analysis of carbon nanotube-based switches. *Journal of Engineering Materials and Technology*, 126:230–237, 2004.

[6] W G Conley, A Raman, C M Krousgrill, and S Mohammadi. Nonlinear and nonplanar dynamics of suspended nanotube and nanowire resonators. *Nano Letters*, 8:1590–1595, 2008.

[7] M-F Yu, G J Wagner, R S Ruoff, and M J Dyer. Realization of parametric resonances in a nanowire mechanical system with nanomanipulation inside a scanning electron microscope. *Physical Review B*, 66:073406, 2002.

[8] T Ouisse, F Martins, M Starck, S Huant, and J Chevrier. Signal amplitude and sensitivity

of the Kelvin probe force microscopy. *Applied Physics Letters*, 88:043102, 2006.

[9] D W Jordan and P Smith. *Nonlinear Ordinary Differential Equations, 3rd Ed.* Oxford, Oxford England, 1999.

[10] E Mathieu. Mémoire sur le mouvement vibratoire dune membrane de forme elliptique. *Journal des Mathématiques Pures et Appliques*, 1:137–203, 1868.

[11] J. F. Rhoads, S. W. Shaw, K. L. Turner, J. Moehlis, B. E. DeMartini, and W. Zhang. Generalized parametric resonance in electrostatically actuated microelectromechanical oscillators. *Journal of Sound and Vibration*, 296(4-5):797–829, 2006.

[12] J F Rhoads, S W Shaw, K L Turner, and R Baskaran. Tunable microelectromechanical filters that exploit parametric resonance. *Journal of Vibration and Acoustics*, 127:423–430, 2008.

[13] C. S. Liu and V. K. Tripathi. Observational consequences of parametrically driven vibrations of carbon nanotubes. *Physical Review B*, 70, 2004.

[14] A. Ahmad and V. K. Tripathi. Parametric excitation of higher-order electromechanical vibrations of carbon nanotubes. *Physical Review B*, 72, 2005.

[15] L Meirovitch. *Principles and Techniques of Vibrations.* Prentice Hall, Upper Saddle River, NJ, 1997.

[16] K L Turner, S A Miller, P G Hartwell, N C MacDonald, S H Strogatz, and S G Adams. Five parametric resonances in a microelectromechanical system. *Nature*, 396:149–152, 1998.

[17] E J Doedel. *AUTO 07P: Continuation and Bifurcation Software for Ordinary Differential Equations.* http://indy.cs.concordia.ca/auto, 2006.

[18] J F Rhoads, S W Shaw, and K L Turner. The nonlinear response of resonant microbeam systems with purely-parametric electrostatic actuation. *Journal of Micromechanics and Microengineering*, 16:890–899, 2006.

[19] A H Nayfeh and D T Mook. *Nonlinear Oscillations.* John Wiley & Sons, 1995.

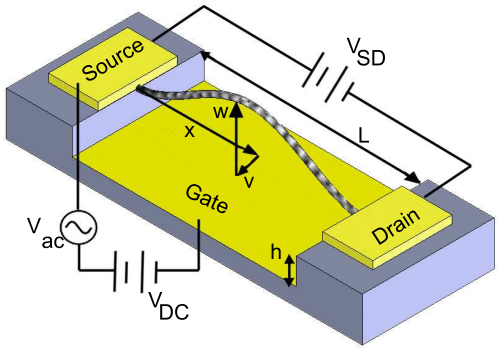

Figure 1: Schematic of a suspended nanotube resonator of length L, and diameter d, suspended above a planar gate electrode separated by gap h. DC and AC excitation voltages are applied to both tune the natural frequency and excite the resonator into periodic oscillations.

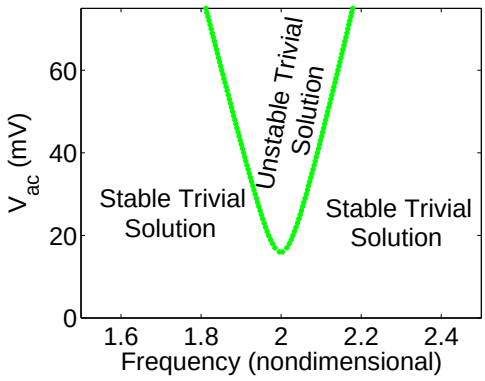

Figure 6: Stability boundary of the purely parametrically excited system ($F_0 = F_2 = 0$) for $V_g^2 \approx 2V_{dc}V_{ac}\sin(\Omega\tau)$. The boundaries are calculated for $V_{dc} = 200$mV. The region centered about $\Omega = 2$ has a non-trivial (non-zero) amplitude; the amplitude response of several specific voltages is shown in Figure 2. Note that $V_{ac} > 15$mV for non-trivial solutions to exist.

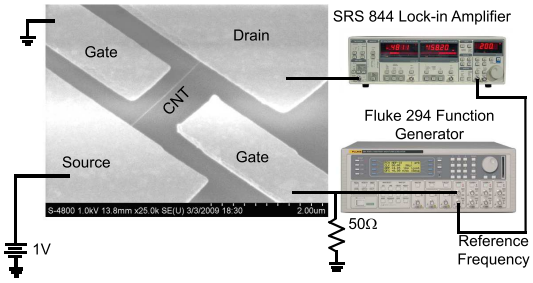

Figure 7: SEM of a SWCNT suspended between two gate electrodes. The suspended CNT is free to vibrate both vertically and horizontally. This measurement detects the motion of the CNT directly instead of depending on a signal down mixing technique as used in previous works.

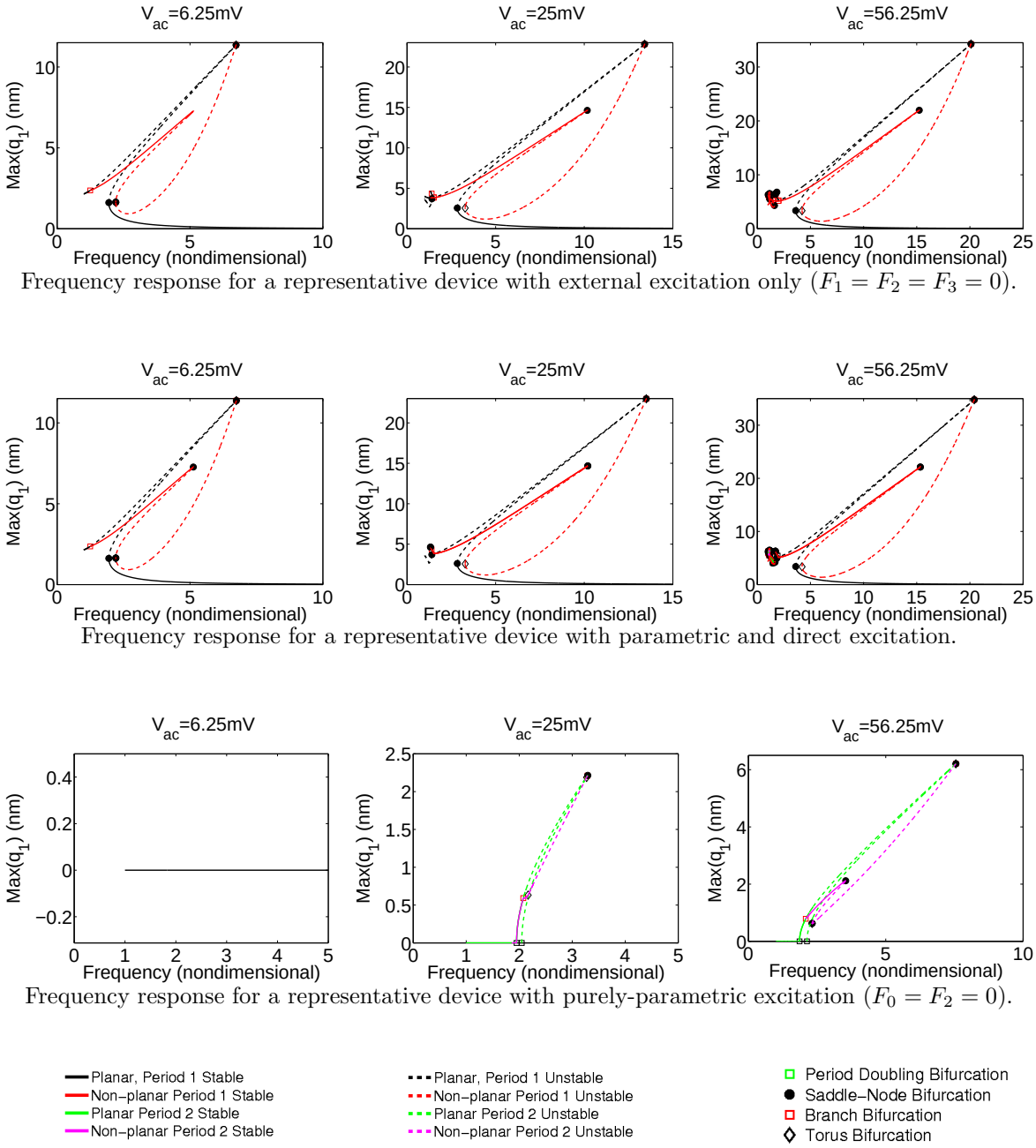

Frequency response for a representative device with external excitation only ($F_1 = F_2 = F_3 = 0$).

Frequency response for a representative device with parametric and direct excitation.

Frequency response for a representative device with purely-parametric excitation ($F_0 = F_2 = 0$).

Figure 2: In-plane amplitude response of Eq. (3) assuming $V_g^2 \approx 2V_{dc}V_{ac}\sin(\Omega\tau)$. Note that the results obtained for the device with external forcing only are nearly identical to the results associated with the complete excitation model. The amplitudes of the parametric resonances are very small under moderate excitation as shown in the 3rd row of the figure.

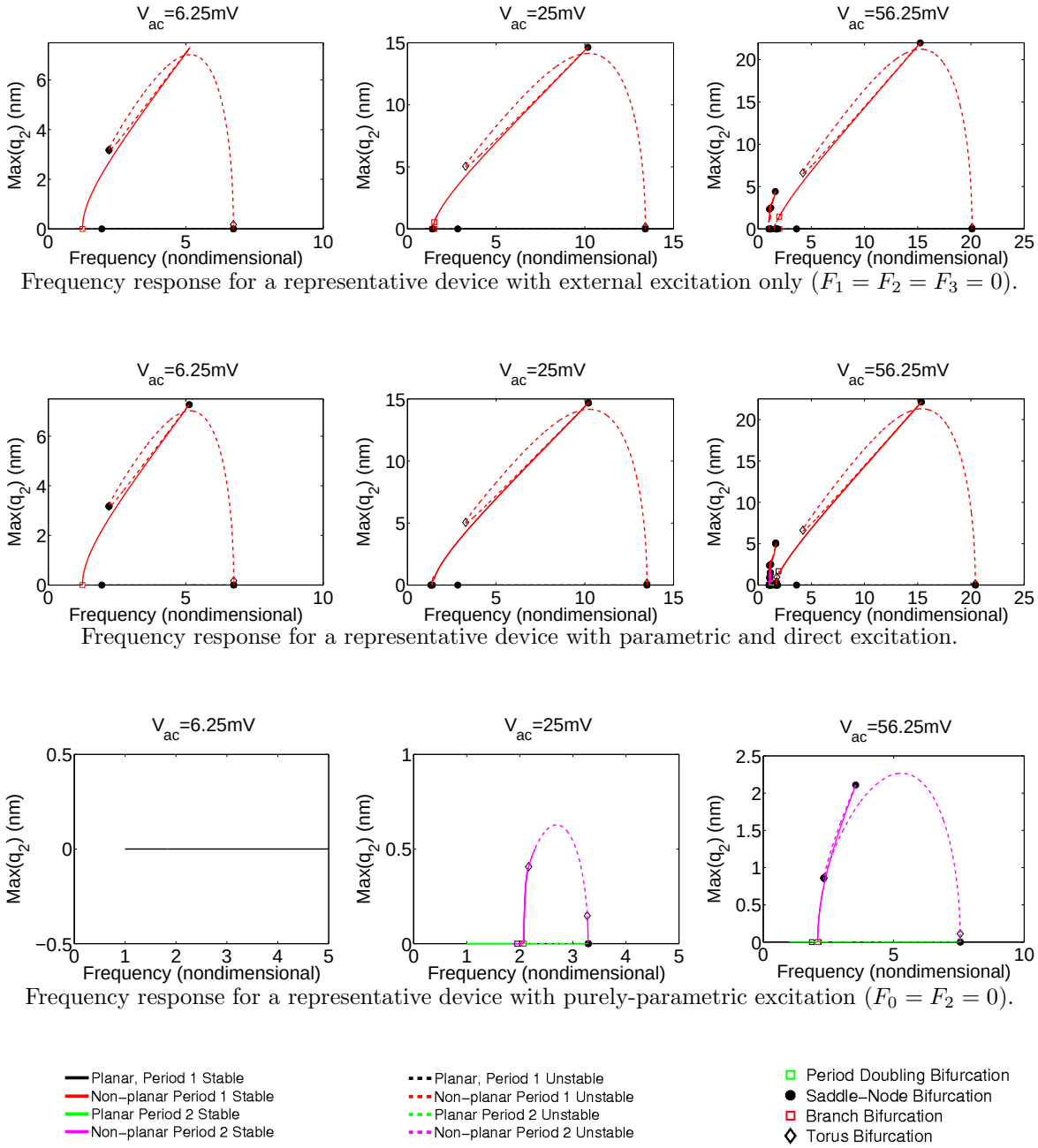

Figure 3: Out-of-plane amplitude response of Eq. (3) assuming $V_g^2 \approx 2V_{dc}V_{ac}\sin(\Omega\tau)$. Note that the results obtained for the device with external forcing only are nearly identical to the results associated with the complete excitation model. The amplitudes of the parametric resonances are very small under moderate excitation as shown in the 3rd row of the figure.

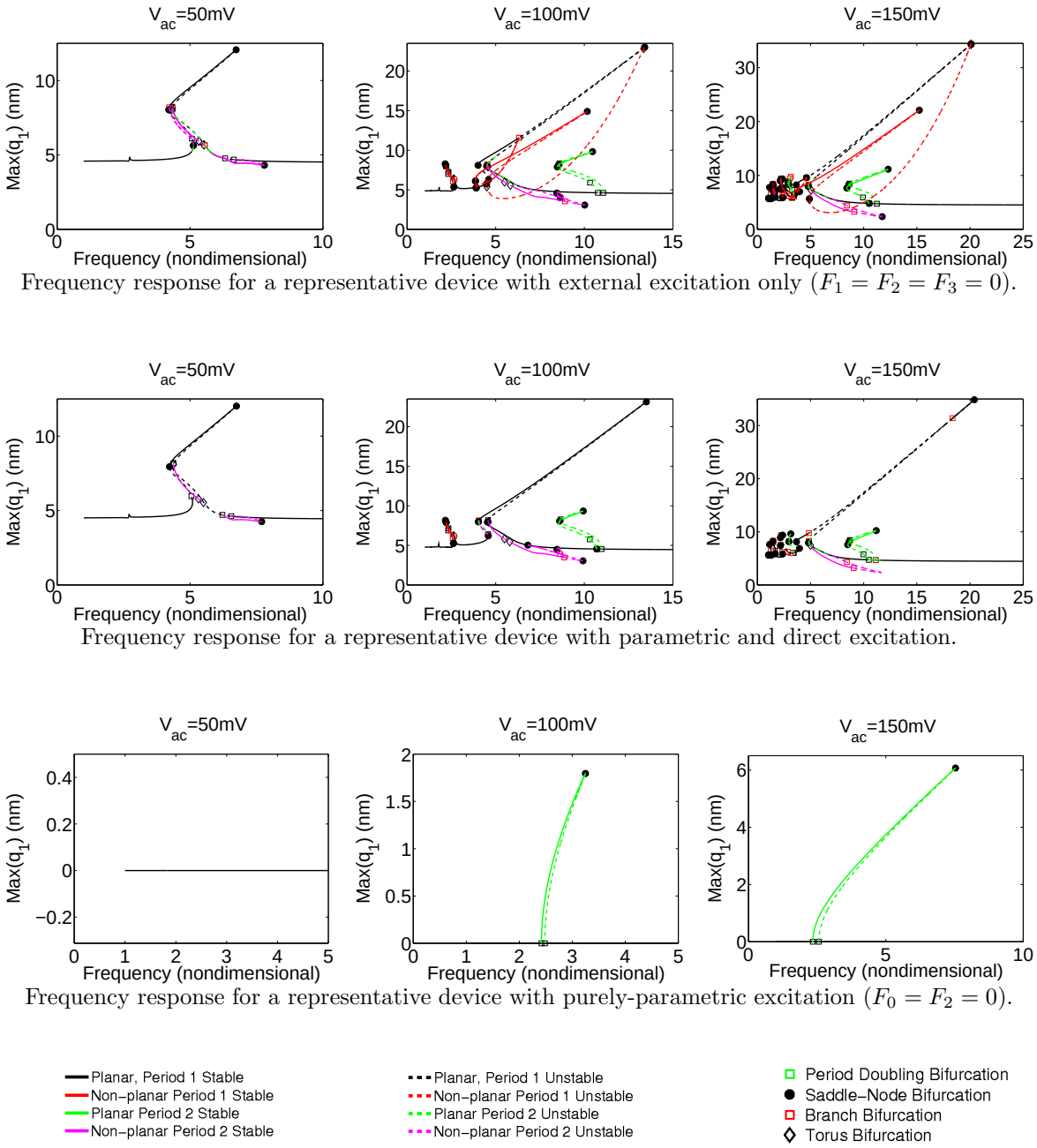

Figure 4: In-plane amplitude response of Eq. (3) assuming $V_g = \sqrt{V_{dc}^2 + V_{ac}^2 sin(\Omega\tau)}$. Note that the results obtained for the device with external forcing only are nearly identical to the results associated with the complete excitation model. The amplitudes of the parametric resonances are very small under moderate excitation as shown in the 3rd row of the figure. Note the AC excitation voltages are selected to match the same magnitude of forcing as used in Figs. 2 and 3.

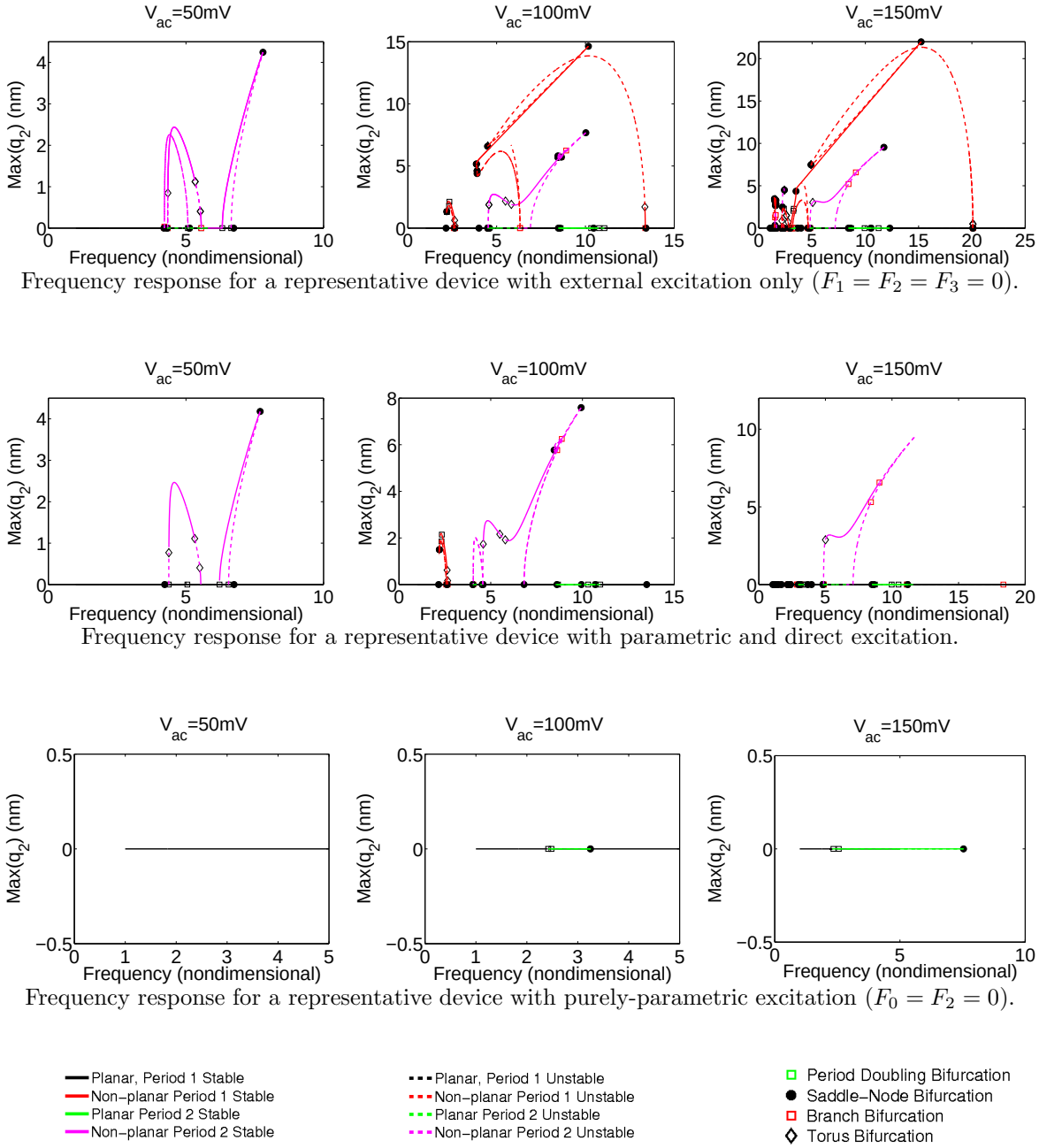

Figure 5: Out-of-plane amplitude response of Eq. (3) assuming $V_g = \sqrt{V_{dc}^2 + V_{ac}^2 \sin(\Omega\tau)}$. Note that the results obtained for the device with external forcing only are nearly identical to the results associated with the complete excitation model. The amplitudes of the parametric resonances are very small under moderate excitation as shown in the 3rd row of the figure.